This article has been accepted for publication in IEEE Transactions on Medical Robotics and Bionics. This is the author's version which has not been fully edited and content may change prior to final publication. Citation information: DOI 10.1109/TMRB.2024.3504003

Preliminary Assessment of Accurate Motion Detection via Magnetic Tracking towards Wearable Technologies

Federico Masiero[†1], *Member, IEEE*, Valerio Ianniciello[†2], Roberto Raeli[2], Edoardo Sinibaldi[*3], *Senior Member, IEEE*, Lorenzo Masia[*1], *Senior Member, IEEE*, Christian Cipriani[*2], *Senior Member, IEEE*

***Abstract*— Tracking permanent magnets represents a low-footprint and passive approach to monitoring objects or human motion by attaching or embedding magnets therein. Recent tracking techniques achieved high-bandwidth detection considering a simplified model for the magnetic sources, i.e. the dipole model. Nonetheless, such a model can lead to inaccurate results any time a non-spherical magnet approaches the sensor array. Here, we present a novel tracking algorithm based on an analytical model for permanent magnet cylinders with uniform arbitrary magnetization. By means of a physical system mounting 20 magnetometers, we compared the tracking accuracy obtained with our algorithm vs. results obtained by using the dipole model and with respect to a ground-truth reference. With a single magnetic target, our algorithm can significantly lower position (up to 0.68 mm) and orientation errors (up to 2.5°) while enabling online tracking (computation time below 19 ms). We also accurately tracked two magnets, by obtaining a reduction in position error (up to 0.92 mm) vs. the dipole-based algorithm. These findings broaden the applicability of accurate magnetic tracking to real-time applications, facilitating the tracking of multiple magnetic targets in proximity of the magnetic sensors. This advancement opens avenues for applications in wearable devices, advancing the field of motion detection beyond traditional inertial measurement units.**

I. INTRODUCTION

Magnetic tracking involves the determination of the position and orientation (namely, the pose) of magnets or coils from the fields they generate. Tracking permanent magnets can offer further advantages over coil-based systems; indeed, in addition to generating stronger fields, magnets are passive markers, which do not require wiring and power. These features found wide applicability in biomedical engineering; indeed, magnets have been adopted to track ingestible capsules [1], surgical instruments [2], or even to monitor artificial and natural organs, such as heart valves [3] and skeletal muscles [4]. Nevertheless, magnetic tracking found use also outside the medical field as an alternative to traditional motion detection technology, e.g. to track fingers motion [5], hand-held tools [6], and joints of wearable robots [7].

Promising methods to track permanent magnets involve the use of statistical filters [8], swarm intelligence and genetic algorithms [9], machine-learning methods [10], or nonlinear optimization [4], [11], [12]. The latter proved to be the most adopted approach for its greater ease of implementation and better scalability to different sensor arrangements and magnets number.

Except for machine-learning methods, magnetic tracking algorithms require a model for the prediction of the magnetic field generated by the sources. When considering cylindrical permanent magnets, analytical models included in tracking algorithms were almost exclusively based on the dipole approximation [13]. Such an approximation, however, is known to provide reliable field estimations only far from the magnets [13], [14]. Motivated by this detrimental limitation, alternative approaches considered FEM models [15], which can successfully provide real-time pose estimation of a single magnet even in proximity of the sensors at the cost of a larger memory management w.r.t. (with respect to) an analytical approach.

A further limitation of the dipole model relies in its axial symmetry, which prevent to estimate magnet rotations around its magnetization axis. However, some magnetized bodies, e.g. diametrically magnetized cylinders, do not generate axial-symmetric fields, so that their poses could be fully estimated, in principle, based on field data. Based on this, numerical modeling of the field was proposed for the full-pose tracking of a diametrically magnetized capsule robot, but results were confined to a simulated environment for the excessive computational burden [16], hardly limiting real-time and embedded applications of such technology.

Here, we present a novel implementation of a very accurate algorithm for simultaneous and online tracking of multiple cylindrical magnets with arbitrary uniform magnetization. The proposed algorithm exploits an exact, singularity-free and computationally cheap analytical model to evaluate the field of uniformly magnetized cylindrical magnets systems [14]. Such an algorithm can be applied to track objects with different magnetization, i.e. either axial or diametric cylinders, allowing to estimate an additional degree of free-

This work was supported in part by the European Research Council under the MYKI Project (ERC-2015-StG, Grant No. 679820) and in part by the European Union's Horizon 2020 Research and Innovation Program under the SCOUT Project (Marie Skłodowska-Curie Grant, Grant No. 101149980) (*Corresponding authors: Federico Masiero and Valerio Ianniciello, e-mails: federico.masiero@ziti.uni-heidelberg.de, valerio.ianniciello@santannapisa.it*).

† F. Masiero and V. Ianniciello equally contributed to this work.

* E. Sinibaldi, L. Masia and C. Cipriani share the senior authorship.

[1] F. Masiero and L. Masia are with the Institut für Technische Informatik (ZITI), Heidelberg University, 69120 Heidelberg, Germany.

[2] V. Ianniciello, R. Raeli and C. Cipriani are with the BioRobotics Institute and the Department of Excellence in Robotics and AI, Scuola Superiore Sant'Anna, 56127 Pisa, Italy.

[3] E. Sinibaldi is with the Istituto Italiano di Tecnologia, 16163 Genoa, Italy.

dom for the latter, hence providing a full pose estimation in terms of Cartesian position and orientation. We tested the performance of our algorithm with a physical system consisting of an array of 20 magnetometers, using up to two axially- and diametrically-magnetized cylindrical magnets, assessing their pose estimates and compared the results with the state-of-the-art tracking algorithm (employing the dipole model). Outcomes suggest that our algorithm outperform the accuracy reached via the dipole model, lowering position and error (up to 0.68 mm and 2.5° of reduction, respectively) when tracking cylindrical magnets in proximity of the sensor array, still exhibiting a low computation time (∼14-19 ms for a single magnet) that allows its online use.

II. MATERIALS AND METHODS

A. Tracking Algorithm

The proposed algorithm is based on nonlinear optimization: magnets pose is iteratively estimated by minimizing a cost function. During each iteration the estimate of magnets pose is used to calculate a predicted magnetic field, $\mathbf{B}_i$, at a number of known sensor locations in the sensor array. Those are compared with the actual magnetic field measurements, $\bar{\mathbf{B}}_i$, to compute a magnetic field prediction error, $\mathbf{E}_i = \bar{\mathbf{B}}_i - \mathbf{B}_i$. Then, magnets pose are determined from the optimization solution (which minimizes $\mathbf{E}_i$) and used as the initial estimate for the subsequent tracking step.

In this algorithm, the pose of the j-th magnet is described through its 3D position $\mathbf{r}_j = (x_j, y_j, z_j)^T$ and its orientation expressed as a unit quaternion $\mathbf{q}_j = (q_{j0}, q_{j1}, q_{j2}, q_{j3})^T$ (with $\|\mathbf{q}_j\| = 1$). Equivalently, the orientation can be described by two magnet axes, namely the main cylinder axis $\hat{\mathbf{e}}_{j\parallel}$ and one of its axes along the cylinder diameter $\hat{\mathbf{e}}_{j\perp}$, which can be related to the quaternion components as:

$$\hat{\mathbf{e}}_{j\parallel} = \begin{bmatrix} 2(q_{j1}q_{j3}+q_{j0}q_{j2}) \\ 2(q_{j2}q_{j3}-q_{j0}q_{j1}) \\ 1-2(q_{j1}^2+q_{j2}^2) \end{bmatrix}, \quad (1)$$

$$\hat{\mathbf{e}}_{j\perp} = \begin{bmatrix} 1-2(q_{j2}^2+q_{j3}^2) \\ 2(q_{j1}q_{j2}+q_{j0}q_{j3}) \\ 2(q_{j1}q_{j3}-q_{j0}q_{j2}) \end{bmatrix}. \quad (2)$$

Calling the position of the i-th sensor $\mathbf{r}_i = (x_i, y_i, z_i)^T$, we can define the distance vector from the j-th magnet to the i-th sensor as $\mathbf{p} = \mathbf{r}_i - \mathbf{r}_j$. Other than $\mathbf{p}$, the field of a magnetic cylinder is specified by its radius (R_j), length (L_j) and magnetization ($\mathbf{M}_j^\star$). For uniformly magnetized cylinders, $\mathbf{M}_j^\star$ can be split in two contributions: one parallel to the cylinder axis $\mathbf{M}_{j\parallel}$, and one perpendicular to it $\mathbf{M}_{j\perp}$, so that $\mathbf{M}_j^\star = \mathbf{M}_{j\parallel} + \mathbf{M}_{j\perp} = \mathrm{M}_{j\parallel}\hat{\mathbf{e}}_{j\parallel} + \mathrm{M}_{j\perp}\hat{\mathbf{e}}_{j\perp}$, with $\hat{\mathbf{e}}_{j\parallel}$ and $\hat{\mathbf{e}}_{j\perp}$ unit vectors corresponding to the axial and diametric directions, respectively. Notably, being purely axial ($\mathbf{M}_j^\star = \mathbf{M}_{j\parallel} = \mathrm{M}_{j\parallel}\hat{\mathbf{e}}_{j\parallel}$) implies that the magnet is axial-symmetric and $\hat{\mathbf{e}}_{j\perp}$ can be any axis orthogonal to $\hat{\mathbf{e}}_{j\parallel}$, confirming that only 5 degrees of freedom (DoF) can be found for this object (akin the point dipole). Conversely, when the magnetic cylinder has a nonzero component of magnetization aligned with $\hat{\mathbf{e}}_{j\perp}$ (that is the case for a diametric cylinder, $\mathbf{M}_j^\star = \mathbf{M}_{j\perp} = \mathrm{M}_{j\perp}\hat{\mathbf{e}}_{j\perp}$), both axes ($\hat{\mathbf{e}}_{j\parallel}$, $\hat{\mathbf{e}}_{j\perp}$) are necessary to describe magnet's orientation (6-DoF pose).

The magnetic field generated at the location $\mathbf{r}_i$ by a uniformly magnetized cylinder with origin in $\mathbf{r}_j$ and magnetization $\mathbf{M}_j^\star$ reads [14]:

$$\mathbf{B}_{ij} = \frac{\mu_0}{\pi}\left(f_1(2\mathbf{M}_{j\parallel} - \mathbf{M}_{j\perp}) + f_2\mathbf{u}_j + f_3\mathbf{v}_j\right) \quad (3)$$

where μ_0 is the vacuum permittivity, and the auxiliary definitions of f_1, f_2, f_3, $\mathbf{u}_j$ and $\mathbf{v}_j$ can be found in [14]. Using Eq. (3), the field prediction at the i-th sensor location $\mathbf{B}_i$, can be estimated from the compound field generated by each individual magnet contribution $\mathbf{B}_{ij}$ at that location.

The tracking algorithm was implemented in MATLAB running the Levenberg-Marquardt algorithm (LMA) via the lsqnonlin built-in solver, minimizing the costs:

$$\mathbf{E}_i = \bar{\mathbf{B}}_i - \mathbf{B}_i = \bar{\mathbf{B}}_i - \sum_j \mathbf{B}_{ij}, \quad 1 - \|\mathbf{q}_j\|^2 \quad (4)$$

where the last term in Eq.(4) is a penalty for $\|\mathbf{q}_j\|$.

For comparison, the same minimization procedure was also run using Eq. (4) with the dipole model. Both algorithms were run online on a Laptop with 8 GB of RAM and an Intel i7 CPU running at 2.3 GHz, employing the magnetic field measurements collected and streamed through serial port (10 Hz) by a single acquisition unit (AU). The AU is a custom printed circuit board mounting 20 three-axis magnetic field sensors (LIS3MDL, STMicroelectronics), arranged on a 4×5 grid with a 9 mm inter-sensor distance [17].

B. Magnets Strength Estimation

Magnet strengths need not be estimated, but their estimation can compensate for errors in the factory specifications of magnets as well as their relationship to sensor gains [11]. The estimation of the magnet strength can be done with the same methodology previously described for magnetic tracking, but this time considering known the magnet position and orientation w.r.t. the sensor array, and searching for the unique parameter $\|\mathbf{M}_j^\star\|$ via nonlinear optimization.

A custom 3D-printed support (printed with an UltiMaker S5, nominal resolution: 50 μm) was used to place the magnet origin ($\mathbf{r}_j$) aligned with the center of the AU at different distances d from it, and with the possibility to orient the magnets along the three main axes of AU ($\mathbf{q}_j$) (Fig. 1A).

We collected the magnetic field data of an axial and a diametric magnet (both having $R = 1$ mm and $L = 10$ mm) positioning their origins at $d = 10, 15, ..., 35$ mm, and orienting the magnets along all the principal axes of the AU. For the diametric magnet, being this non-symmetric for its magnetization direction, we also used an angular reference during the placement. Then, the whole set of data was used to run LMA offline, and the median estimated value of $\|\mathbf{M}_j^\star\|$ for both magnets was then considered for the subsequent tracking experiments.

This article has been accepted for publication in IEEE Transactions on Medical Robotics and Bionics. This is the author's version which has not been fully edited and content may change prior to final publication. Citation information: DOI 10.1109/TMRB.2024.3504003

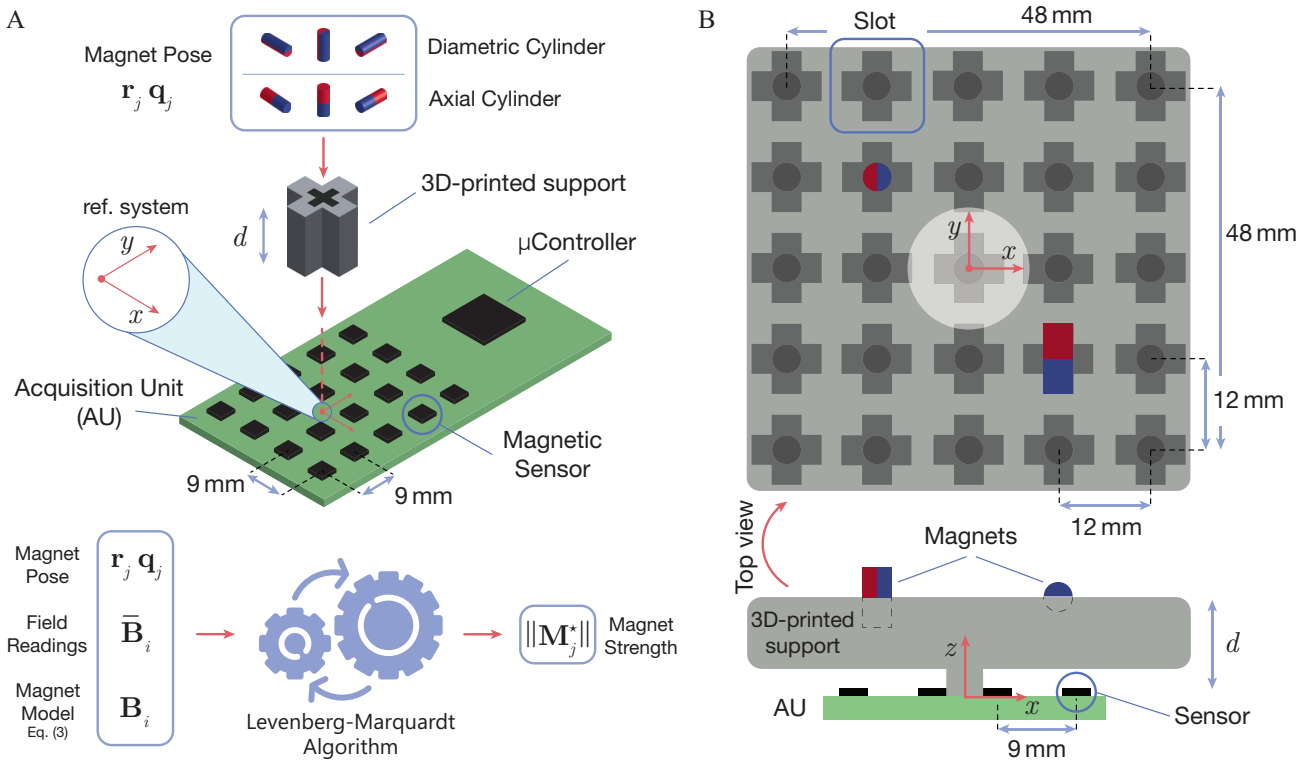

Fig. 1. (**A**) Overview of the system setup for the estimation of magnets strength. A 3D frame was used to place the magnet with known position $\mathbf{r}_j$ and orientation $\mathbf{q}_j$ w.r.t. the AU, at increasing distances d and aligned with the AU center. Magnetic field data were recorded for each magnet for all magnets orientations and at distances $d = 10, 15, ..., 35$ mm. Data were processed offline running LMA through the lsqnonlin solver, providing as input $\mathbf{r}_j$, $\mathbf{q}_j$, and fitting the magnetic field data with Eq. (3) to extract the magnet strength $\|\mathbf{M}_j^\star\|$. (**B**) Setup of tracking experiments, which included an acquisition unit (AU) and a 3D-printed support for (*i*) precise positioning of the magnets at various distances from the sensors (d from 10 mm to 35 mm, with 5 mm step) and (*ii*) magnet orientation along the three principal axes of the AU.

C. Experiments

Our tracking algorithm was validated using a custom 3D-printed support to precisely place magnets w.r.t. the AU within a centered volume grid of size $48\times48\times25$ mm^3, with 12 mm grid step along the x and y, while allowing 5 mm grid step along z. With this frame the magnet can be positioned with the cylinder axis aligned with all the three Cartesian axes of the AU reference system (Fig. 1B).

We characterized the performance of our algorithm against our previous desktop implementation using the dipole model [12], using two NdFeB cylinders ($R = 1$ mm, $L = 10$ mm, N48), one with axial and the other with diametric magnetization. Before tracking, the AU was calibrated by measuring the average disturbing fields (in absence of magnets in the workspace) to compensate for the geomagnetic field and sensors offsets. After calibration, one of the two magnets was placed in a slot of the support and tracked online using the magnetic field data streamed by the AU to the Laptop. For each magnet placement the median tracked pose over a 2 s acquisition was stored. This procedure was repeated for each of the 25 available slots, placing the magnet aligned with all three principal axes of the AU, for a total of 75 data samples per plane. Tests were performed at six distances from the AU, i.e. from 10 mm to 35 mm with a 5 mm step.

The capability of the algorithm in simultaneously tracking two magnets was also characterized using either 2 axial magnets or 2 diametric magnets. Similar to the one-magnet tests, the AU was calibrated first to compensate for the geomagnetic field and sensors offsets. After calibration, both magnets were positioned in the 3D-printed support at 21 planar random positions and orientations (with the only constraint of not being placed in adjacent slots), and tracked online using the magnetic field data streamed by the AU to the Laptop. For each magnets placement the median tracked poses over a 2 s acquisition were stored. Tests were performed for three distances from the sensor array, i.e. 15, 20, 25 mm.

D. Performance Metrics

Position accuracy was evaluated as the norm of the difference between the known position ($\mathbf{p}_j$, from the 3D-CAD model) and the estimated one ($\bar{\mathbf{p}}_j$) with both tracking algorithms (using our algorithm and the one with the dipole model):

$$E_d = \|\mathbf{p}_j - \bar{\mathbf{p}}_j\| \tag{5}$$

Similarly, orientation accuracy was evaluated computing the angular offset (orientation error) between the known unit magnetization vector ($\mathbf{M}_j^\star$) and the estimated one ($\bar{\mathbf{M}}_j^\star$):

$$E_{oM} = \cos^{-1}\left(\mathbf{M}_j^\star \cdot \bar{\mathbf{M}}_j^\star \,/\, \|\mathbf{M}_j^\star\|\|\bar{\mathbf{M}}_j^\star\|\right) \tag{6}$$

This article has been accepted for publication in IEEE Transactions on Medical Robotics and Bionics. This is the author's version which has not been fully edited and content may change prior to final publication. Citation information: DOI 10.1109/TMRB.2024.3504003

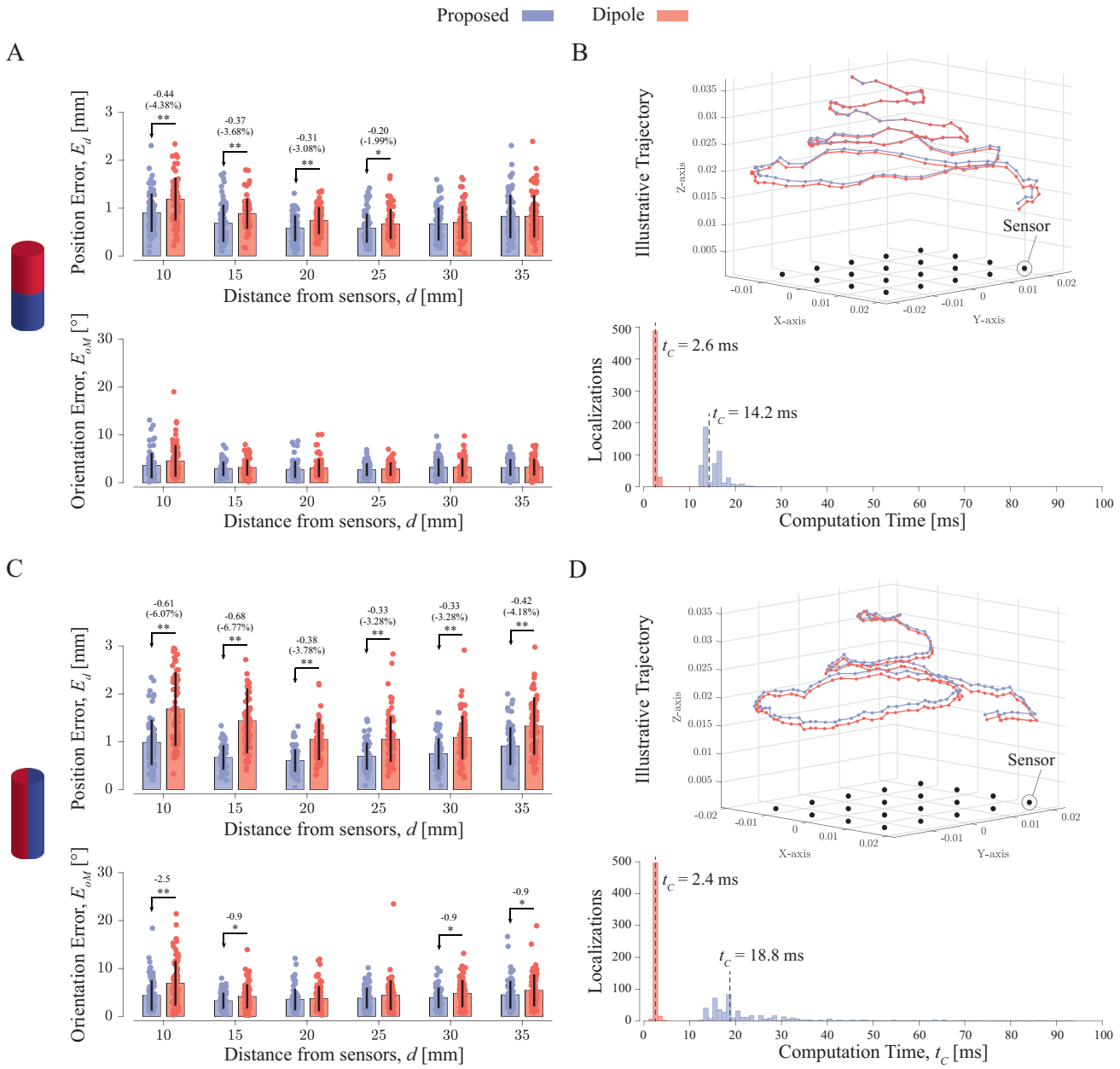

Fig. 2. Position (E_d) and orientation (E_{oM}) errors of the proposed algorithm (blue) vs. the dipole one (red) for a single axial (A) or diametric (C) magnet at different distances from the sensors (d). Significant differences (Wilcoxon test) performed on E_d and on E_{oM} are reported with (*) and (**), for $p < 0.05$ and $p < 0.01$, respectively. Difference in position error is also reported, both in absolute terms and relative (%) to the magnet characteristic size $r^\star$. Illustrative trajectory, tracked with both the dipole and proposed algorithm, of a single slowly moving axial (B) and diametric (D) magnets, with corresponding computation times t_C (over $>$ 10s of recording).

When tracking diametric magnets using our algorithm, we also evaluated the angular offset between the estimated ($\hat{\mathbf{e}}_{j\parallel}$) and tracked cylinder axis ($\bar{\hat{\mathbf{e}}}_{j\parallel}$):

$$E_{oA} = \cos^{-1}\left(\hat{\mathbf{e}}_{j\parallel} \cdot \bar{\hat{\mathbf{e}}}_{j\parallel}\right) \tag{7}$$

The computation times, t_C, of the two implementations of the magnetic tracking algorithms when tracking a single moving magnet were also stored for further analyses.

E. Statistical Analysis

The normality of the distributions of E_d and E_{oM} was verified with the Shapiro–Wilk test (significance level, $\alpha = 0.05$). One-tail Wilcoxon signed-rank test ($\alpha = 0.05$) was used to assess the statistical significance between errors distribution (proposed method vs. the dipole one).

III. RESULTS

The magnetic strength was estimated to be 868 ± 6 kA/m (mean $\pm$ standard deviation) and 809 ± 11 kA/m for the axial and the diametric magnet, respectively. Those values exhibited minimal variability and were robust to magnet positioning (distance and orientation).

The proposed algorithm generally proved more accurate

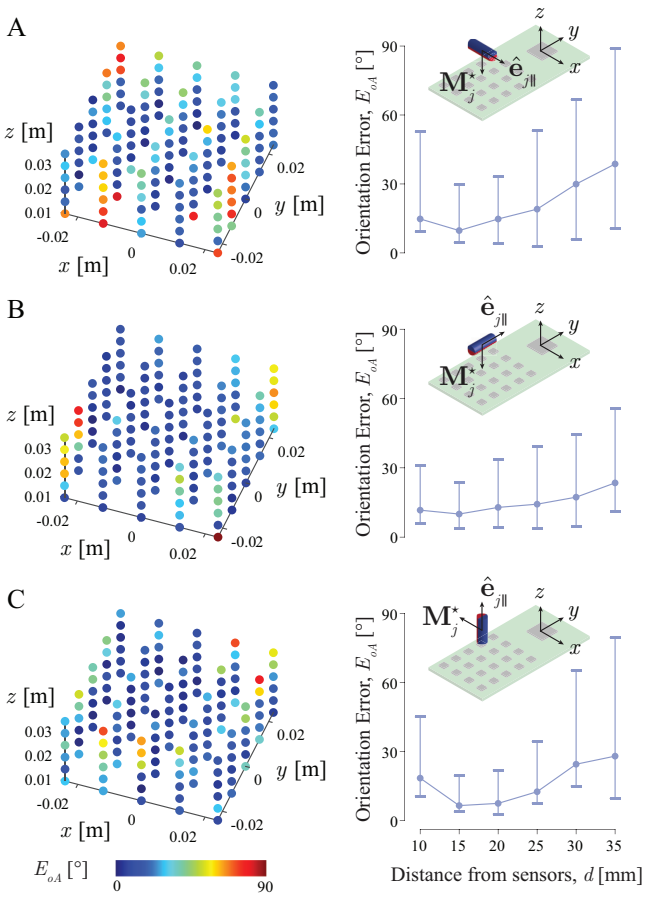

Fig. 3. Orientation accuracy in estimating the cylinder axis $\hat{\mathbf{e}}_{j\parallel}$ for a diametric cylindrical magnet oriented in three different configuration w.r.t. the AU: (A) with $\hat{\mathbf{e}}_{j\parallel}$ parallel to the AU's x axis, (B) with $\hat{\mathbf{e}}_{j\parallel}$ parallel to the AU's y, (C) with $\hat{\mathbf{e}}_{j\parallel}$ perpendicular to the AU. In the scatter plots (left column) the orientation is color-coded in correspondence of the tested magnet locations. The corresponding right plots render the median and inter-quartile range of the errors for all the considered distance values.

than the one employing the dipole model (Fig. 2). At all distances and for both magnets type, the average position E_d and orientation E_{oM} errors of our algorithm proved below or equal to 1 mm and 5°, respectively (vs. 1.7 mm and 7.5° of the dipole model). Specifically, when tracking an axial magnet (Fig. 2A), our approach exhibited lower E_d than the dipole one ($p < 0.05$) up to 25 mm far from the AU, with higher differences observed close to the sensors (E_d was reduced from only 0.2 mm at $d = 25$ mm distance, up to 0.44 mm at $d = 10$ mm). Conversely, no significant difference was found for the E_{oM}. Instead, when tracking a diametric magnet (Fig. 2C), our approach exhibited lower E_d than the dipole one ($p < 0.05$) at all the tested distances. Similarly to the axial case, larger E_d reduction were observed at close distances from the sensors, i.e. at $d = 10$ and 15 mm (for which reductions were about 0.61 mm and 0.68 mm, respectively). For a diametric magnet, also E_{oM} proved significantly lower ($p < 0.05$) at close (≤ 15 mm) and far (≥ 30 mm) distances, with a reduction of the orientation error comprised between 0.9° and 2.5°. For ease of readability, difference in position error is also reported in the bar plots in Fig. 2A,C, both in absolute and relative terms (by assuming as reference length the radius of the minimum bounding sphere for the considered magnet, namely $r^\star = \sqrt{101}$ mm).

A qualitative comparison of the two algorithms when tracking a spiral trajectory performed by hand highlighted that the use of the dipole model introduced a larger error along the vertical direction (especially) in proximity of the sensors (Fig. 2B,D). When tracking a diametric cylinder, this error is maintained at all distances and a distinguishable tracking difference between the approaches was observed even at 30 mm from the sensors. Remarkably, the two computation times t_C were sensibly different: tracking with the dipole model took around 2.4-2.6 ms, while our algorithm took around 14.2-18.8 ms (Fig. 2B,D).

The tracking accuracy of the cylinder axis E_{oA} for a single diametric magnet sensibly varied depending on the testing conditions, which included: magnet orientation, placement on the 3D-support, and distance from the sensors, d (Fig. 3). In general, best results were found at $d = 15, 20$ mm distance, for which the median orientation error was less than 15°. Results worsen for increasing d and when placing the magnets towards the AU boundaries, exhibiting more than 30° of median error and large variability.

When simultaneously tracking two cylindrical magnets, significant differences were found when tracking two diametric magnets 4), as both magnets showed smaller E_d at $d = 15, 20$ mm distance ($p < 0.01$), while only one of the two showed smaller E_d at $d = 25$ mm ($p < 0.05$). The obtained significant difference for the case of diametric magnetization, which is the one more challenging and less accomplished by previous investigations, confirms the potential for effective application of the proposed tracking strategy.

IV. DISCUSSIONS & CONCLUSIONS

Incorporating magnetic tracking in motion detection applications represents a promising avenue for advancing the field beyond traditional inertial measurement units. Diverse applications can be foreseen based on this technology. Focusing on the wearable robotics field, embedding magnets in exosuit design can revolutionize gait assistance, posture monitoring, and provide enhanced feedback for fine motor skills. In gait assistance and correction, magnetic markers could enable real-time detection of limb movements, facilitating adaptive support for users with mobility impairments. This technology could also be leveraged for posture monitoring, e.g. to track the torso's orientation and enabling dynamic adjustments in exosuits to support proper postures in occupational settings. Last but not least, in tasks requiring fine motor skills (e.g., surgery, intricate assembly), magnetic markers may offer rich information on hand and finger positioning, contributing to enhance precision and control in exogloves.

Our goal was to develop a novel tracking algorithm with improved accuracy w.r.t. methods employing the dipole model. For the purpose, we included an exact and computationally fast analytical model for cylindrical magnets [14] in the LMA and we experimentally assessed it with a physical

This article has been accepted for publication in IEEE Transactions on Medical Robotics and Bionics. This is the author's version which has not been fully edited and content may change prior to final publication. Citation information: DOI 10.1109/TMRB.2024.3504003

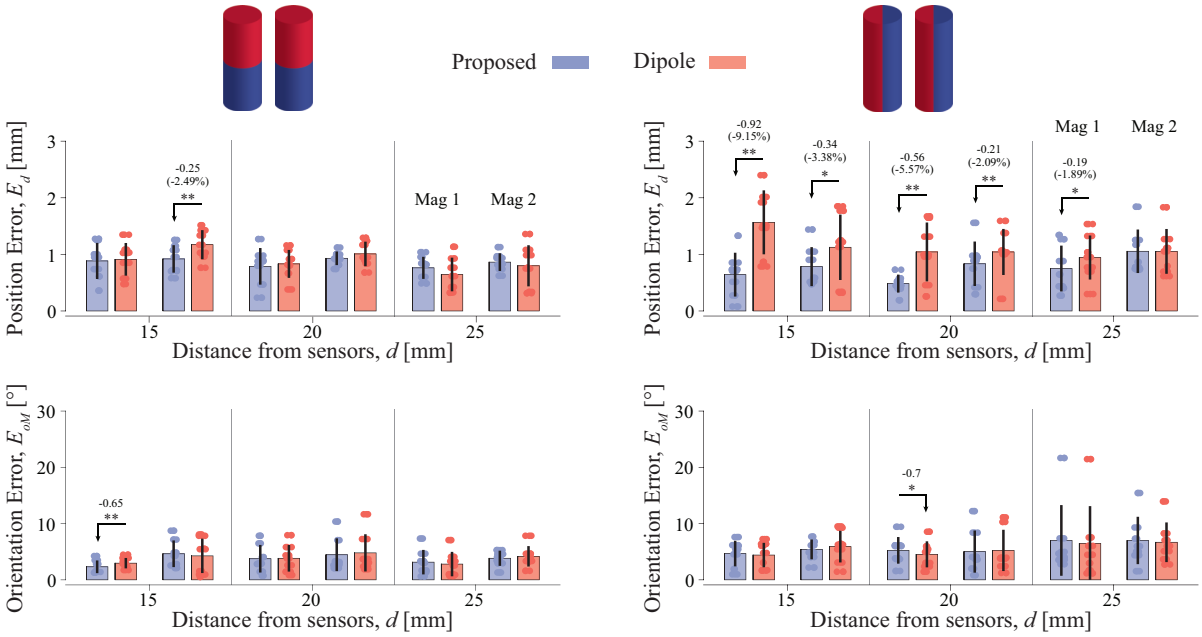

Fig. 4. Position (E_d) and orientation (E_{oM}) errors of the proposed algorithm (blue) vs. the dipole one (red) for two simultaneously tracked axial (A) or diametric (B) magnets at different distances from the sensors (d). Significant differences (Wilcoxon test) performed on E_d and on E_{oM} are reported with (*) and (**), for $p < 0.05$ and $p < 0.01$, respectively. Difference in position error is also reported, both in absolute terms and relative (%) to the magnet characteristic size $r^\star$.

system [17]. Although our results are preliminary and mostly confined to a static/quasi-static assessment, this work already demonstrates the feasibility of simultaneously tracking up to two cylindrical magnets with higher accuracy than previous implementations [12], [11], [17].

As expected, the largest accuracy improvement of our algorithm was observed with diametric cylinders, which have a worse agreement with the dipole compared to axial cylinders [13]. Remarkably, our algorithm was also able to fully estimate the pose, i.e., all the six degrees of freedom of a diametric magnet (Fig. 3), although the resulting accuracy of the estimation showed some variability across the consider test cases.

To the best of our knowledge, this study represents the first physical implementation of a system capable to track (*i*) more than one magnet online (Fig. 4) without using the dipole model and (*ii*) all the six degrees of freedom of a cylindrical marker (thus extending [16]). The algorithm provides outputs in less than 20 ms, which is a significantly shorter time frame compared to related implementations [16]. The current computation time is adequate for real-time tracking across a variety of applications, including those involving human interaction such as controlling wearable devices, tracking human movement, and augmented or virtual reality. Although its speed remains sensibly lower than the algorithm utilizing the dipole model (Fig. 2B,D), deploying this algorithm to an embedded target, could significantly lower its latency. Thus, future work will be dedicated to the embedded implementation of the proposed algorithm, focusing on its real-time implementation possibly exploiting the analytical computation of the derivatives of Eq. (4). This will open the possibility to extensively characterize the dynamic performance of the tracker (which was outside the present scope), and to test it in wearable settings by also considering larger workspaces.

This study was limited in considering a small number of magnets (up to 2) and a unique geometry ($R = 1$ mm, $L = 10$ mm), thus a geometric aspect ratio for which the dipole approximation is challenged. A more thorough characterization considering different geometries and spatial arrangements closer to real-world applications is needed in order to provide a stronger claim on the performance and application range of our algorithm. Future investigations will also address the potential effects of sensor characteristics (such as sampling frequency and resolution [18]), as well as temperature fluctuations and additional magnetic disturbances.

It should be noted that the proposed algorithm is also capable of tracking cylindrical magnets with non-uniform magnetization directions, not limited to alignment with the magnet's principal axes. This capability enables future development of customized cylindrical magnetic markers and systems with specifically programmed magnetization directions [14]. Such systems would be then accurately tracked in real-time using this algorithm.

This work may be of interest for various applications that require proximity tracking of cylindrical magnets with customizable magnetizations. Moreover, it also underscores the transformative potential of magnetic tracking in diverse domains of exosuit technology, paving the way for enhanced functionality and user support.

REFERENCES

[1] G. Ciuti, P. Valdastri, A. Menciassi, and P. Dario, "Robotic magnetic steering and locomotion of capsule endoscope for diagnostic and surgical endoluminal procedures," *Robotica*, vol. 28, no. 2, pp. 199–207, 2010.

[2] Y. Kim, E. Genevriere, P. Harker, J. Choe, M. Balicki, R. W. Regenhardt, J. E. Vranic, A. A. Dmytriw, A. B. Patel, and X. Zhao, "Telerobotic neurovascular interventions with magnetic manipulation," *Science Robotics*, vol. 7, no. 65, p. eabg9907, 2022.

[3] J. A. Baldoni and B. B. Yellen, "Magnetic tracking system: Monitoring heart valve prostheses," *IEEE transactions on magnetics*, vol. 43, no. 6, pp. 2430–2432, 2007.

[4] S. Tarantino, F. Clemente, D. Barone, M. Controzzi, and C. Cipriani, "The myokinetic control interface: tracking implanted magnets as a means for prosthetic control," *Scientific reports*, vol. 7, no. 1, pp. 1–11, 2017.

[5] K.-Y. Chen, S. N. Patel, and S. Keller, "Finexus: Tracking precise motions of multiple fingertips using magnetic sensing," in *Proceedings of the 2016 CHI Conference on Human Factors in Computing Systems*, 2016, pp. 1504–1514.

[6] T. Langerak, J. J. Zárate, D. Lindlbauer, C. Holz, and O. Hilliges, "Omni: Volumetric sensing and actuation of passive magnetic tools for dynamic haptic feedback," in *Proceedings of the 33rd Annual ACM Symposium on User Interface Software and Technology*, 2020, pp. 594–606.

[7] M. Fontana, F. Salsedo, and M. Bergamasco, "Novel magnetic sensing approach with improved linearity," *Sensors*, vol. 13, no. 6, pp. 7618–7632, 2013.

[8] J. Montero, M. Gherardini, F. Clemente, and C. Cipriani, "Comparison of online algorithms for the tracking of multiple magnetic targets in a myokinetic control interface," in *2020 IEEE International Conference on Robotics and Automation (ICRA)*. IEEE, 2020, pp. 2770–2776.

[9] W. Yang, C. Hu, M. Li, M. Q. H. Meng, and S. Song, "A new tracking system for three magnetic objectives," *IEEE Transactions on Magnetics*, vol. 46, no. 12, pp. 4023–4029, 2010.

[10] S. P. Mendez, M. Gherardini, G. V. de Paula Santos, D. M. Muñoz, H. V. H. Ayala, and C. Cipriani, "Data-driven real-time magnetic tracking applied to myokinetic interfaces," *IEEE Transactions on Biomedical Circuits and Systems*, vol. 16, no. 2, pp. 266–274, 2022.

[11] C. R. Taylor, H. G. Abramson, and H. M. Herr, "Low-latency tracking of multiple permanent magnets," *IEEE Sensors Journal*, vol. 19, no. 23, pp. 11 458–11 468, 2019.

[12] F. Clemente, V. Ianniciello, M. Gherardini, and C. Cipriani, "Development of an embedded myokinetic prosthetic hand controller," *Sensors*, vol. 19, no. 14, p. 3137, 2019.

[13] A. J. Petruska and J. J. Abbott, "Optimal permanent-magnet geometries for dipole field approximation," *IEEE transactions on magnetics*, vol. 49, no. 2, pp. 811–819, 2012.

[14] F. Masiero and E. Sinibaldi, "Exact and computationally robust solutions for cylindrical magnets systems with programmable magnetization," *Advanced Science*, vol. 10, no. 25, p. 2301033, 2023.

[15] C. Di Natali, M. Beccani, N. Simaan, and P. Valdastri, "Jacobian-based iterative method for magnetic localization in robotic capsule endoscopy," *IEEE Transactions on Robotics*, vol. 32, no. 2, pp. 327–338, 2016.

[16] S. Song, B. Li, W. Qiao, C. Hu, H. Ren, H. Yu, Q. Zhang, M. Q.-H. Meng, and G. Xu, "6-d magnetic localization and orientation method for an annular magnet based on a closed-form analytical model," *IEEE Transactions on Magnetics*, vol. 50, no. 9, pp. 1–11, 2014.

[17] V. Ianniciello, M. Gherardini, and C. Cipriani, "Transcutaneous magnet localizer for a self-contained myokinetic prosthetic hand," *IEEE Transactions on Biomedical Engineering*, 2023.

[18] F. Masiero, E. Sinibaldi, F. Clemente, and C. Cipriani, "Effects of sensor resolution and localization rate on the performance of a myokinetic control interface," *IEEE Sensors Journal*, vol. 21, no. 20, pp. 22 603–22 611, 2021.